eNeuro

*Research Article: New Research | Development*

# EphrinA5 signaling is required for the distinctive targeting of raphe serotonin neurons in the forebrain.

EphrinA signaling directs serotonin raphe projections

**Teng Teng[1,2,3], Afsaneh Gaillard[4,5], Aude Muzerelle[1,2,3] and Patricia Gaspar[1,2,3]**

[1]*Inserm UMR-S 839, 75005, Paris, France*
[2]*Université Pierre et Marie Curie, Paris, France*
[3]*Institut du Fer à Moulin, Paris, France*
[4]*Inserm 1084, Poitiers, France*
[5]*Université de Poitiers, Poitiers, France*

DOI: 10.1523/ENEURO.0327-16.2017

Received: 9 December 2016

Accepted: 6 January 2017

Published: 26 January 2017

**Author contributions: T.T. and P.G. designed research; T.T. and A.M. performed research; T.T., A.G., and P.G. analyzed data; T.T. and P.G. wrote the paper; A.G. contributed unpublished reagents/analytic tools.**

**Funding:** China Scholarship Council (CSC)
501100004543

**Funding:** Fondation de la Recherche Médicale

**Funding:** Agence Nationale de la Recherche (ANR)
501100001665
ANR-11-0004-02

**Funding:** Institut National de la Santé et de la Recherche Médicale (Inserm)
501100001677

**Funding:** université Pierre et Marie Curie

**The authors declare no competing financial interests.**

Dr Teng Teng was financed by the China Scholarsip Council; Research was supported by the Fondation de la Recherche Médicale and the Investissements d'Avenir program ( ANR-11-0004-02), the Inserm, and the Université Pierre et Marie Curie. The team is part of the Ecole des Neurosciences de Paris training network and of the Bio-Psy Labex.

**Correspondence should be addressed to** Patricia Gaspar, INSERM U 839, 17 rue du Fer à Moulin, 75005, Paris, France. Tel: 331 45 87 61 28 Fax: 331 45 87 61 30. Email: patricia.gaspar@inserm.fr

**Cite as:** eNeuro 2017; 10.1523/ENEURO.0327-16.2017

**Title:** EphrinA5 signaling is required for the distinctive targeting of raphe serotonin neurons in the forebrain.

**Abbreviated title:** EphrinA signaling directs serotonin raphe projections

**Author names affiliations:**

Teng Teng [1, 2,3], Afsaneh Gaillard [4, 5], Aude Muzerelle[1, 2,3], Patricia Gaspar[1, 2,3]

1. Inserm UMR-S 839, 75005, Paris, France

2. Université Pierre et Marie Curie, Paris, France

3. Institut du Fer à Moulin, Paris, France

4. Inserm 1084, Poitiers, France

5. Université de Poitiers, Poitiers, France

**Corresponding author:**

Patricia Gaspar, email: patricia.gaspar@inserm.fr

Address: INSERM U 839, 17 rue du Fer à Moulin, 75005, Paris, France

Tel: 331 45 87 61 28 Fax: 331 45 87 61 30;

**Manuscript information:**

-Number of Figures: 8

-Number of tables: 4

-Number of words in Abstract: 250; Introduction: 510; Discussion : 1534

**Acknowledgements:** We thank Michael Reber for the primers and EphrinA3 construct and for his helpful advice on the manuscript. Imane Moutkine provided essential help for the molecular constructs and for QPCR analyses. Sebastian Brot and Yohan Bertelle are acknowledged for animal breeding, and the IFM imaging facility for advice. Alexandra Rebsam, Sophie Scotto, Anne Teissier, and Mariano Soiza Reilly contributed thoughtful remarks on the project and on the manuscript.

**Conflict of Interest:** The authors declare no competing financial interests.

**Funding sources**: Dr Teng Teng was financed by the China Scholarsip Council; Research was supported by the Fondation de la Recherche Médicale and the Investissements d'Avenir program ( ANR-11-0004-02), the Inserm, and the Université Pierre et Marie Curie. The team is part of the Ecole des Neurosciences de Paris training network and of the Bio-Psy Labex.

## Abstract

Serotonin (5-HT) neurotransmission in the brain relies on a widespread axon terminal network originating from the hindbrain raphe nuclei. These projections are topographically organized such that the dorsal (DR), and median raphe (MnR) nuclei have different brain targets. However, the guidance molecules involved in this selective targeting in development are unknown. Here, we show the implication of ephrinA5 signaling in this process. We find that the *EphA5* gene is selectively expressed in a subset of 5-HT neurons during embryonic and postnatal development. Highest co-expression of *EphA5* and of the 5-HT marker Tph2 is found in the DR with lower co-expression in the MnR, and hardly any colocalization in the caudal raphe in the medulla. Accordingly, ephrinA induced a dose-dependent collapse response of 5-HT growth cones cultured from rostral but not caudal raphe. Ectopic expression of ephrinA3, after in utero electroporation in the amygdala and piriform cortex, repelled 5-HT raphe fiber ingrowth. Conversely, misplaced DR 5-HT axons were found in ephrin A5 KO mice in brain regions that are normally only targeted by MnR 5-HT axons. This causes an overall increase in the density of 5-HT innervation in the ventromedial hypothalamus, the suprachiasmatic nucleus and the olfactory bulb. All these brain areas have high expression of ephrinAs at the time of 5-HT fiber ingrowth. Present results show for the first time the role of a guidance molecule for the region-specific targeting of raphe neurons. This has important implications to understand how functional parsing of central 5-HT neurons is established during development.

**Significance statement:** Present results demonstrate a new role of ephrinA signaling for the selective targeting of 5-HT raphe nuclei. The tyrosine kinase EphA5 is differentially expressed across 5-HT neurons from the different raphe nuclei in mice, correlating with a different repulsive action of ephrinA on the growth of 5-HT axons. EphrinA5 loss of function causes a mis-targeting of dorsal raphe 5-HT axons, whereas overexpression of ephrinA inhibits the ingrowth of 5-HT raphe axons in the amygdala and piriform cortex that are main targets of the dorsal raphe 5-HT neurons. Thus Eph-ephrin signaling acts as a repulsive signal to differentially target 5-HT axons originating from different raphe nuclei.

## Introduction

Serotonin (5-Hydroxytryptamine, 5-HT) neurotransmission is implicated in a large number of physiological functions raising the question of a division of labor among the different hindbrain nuclei that synthesize 5-HT (Calizo et al., 2011; Hale and Lowry, 2011; Kiyasova and Gaspar, 2011). The 5-HT synthesizing neurons are distributed into several raphe nuclei in the hindbrain that have been parsed according to anatomical and physiological criteria. Individual raphe nuclei target different brain regions and consequently, are involved in different functions. For instance the caudal 5-HT raphe nuclei (the B1-B3 cell groups) that are located in the medulla, project to the brainstem and spinal cord are implicated in motor control and in neurovegetative functions (Schmidt and Jordan, 2000; Pflieger et al., 2002; Brust et al., 2014). Conversely, 5-HT neurons of the rostral raphe which are located in the pontine region of the hindbrain (the B5-B9 cell groups) project to the forebrain and have been involved in diverse higher brain functions, such as mood, learning and diverse social behaviors, such as aggression and maternal behavior (Deakin and Graeff, 1991; Lucki, 1998; Fernandez and Gaspar, 2012, Trowbridge et al. 2011). Within these broad raphe divisions, further anatomical and functional distinctions can be made ; for instance the rostral raphe cluster comprises neurons of the dorsal raphe (DR =B6+B7) and the median raphe (MnR= B5+B8) groups that are implicated in different brain functions (Jacobs and Azmitia, 1992; Fernandez et al., 2015; Teissier et al., 2015) and innervate complementary targets in the telencephalon (Vertes et al. 99, Muzerelle et al., 2016). This organization suggests that specific axon guidance molecules could orient the 5-HT-containing axons to specific targets, although the underlying molecular mechanisms are largely unknown (Kiyasova and Gaspar, 2011).

Previous transcriptome profiling of developing 5-HT raphe neurons identified distinct expression profiles between the rostral pontine and the caudal medullary raphe cell groups (Wylie et al., 2010). Among these differentially expressed genes a number of axon guidance molecules, such as Eph receptors and their ephrin ligands are potential candidates for the selective guidance of 5-HT neuron subsets. The properties of EphA receptors as short-range guidance factors make them attractive candidates for selective axon targeting (O'Leary and Wilkinson, 1999; Klein and Kania, 2014). Eph-ephrin signaling has indeed been involved in many functions, one of the best known being it's role for establishing topographic maps in several sensory systems (Prakash et al., 2000; Miko et al., 2007). Moreover the EphA ligand, ephrinA5 was suggested to be involved in the de-

velopment of the dopaminergic neurons, based on its dynamic developmental expression patterns (Deschamps et al., 2009, 2010; Prestoz et al., 2012).

In the present study, we demonstrate a role for Eph-ephrinA signaling in developing 5-HT raphe neurons to repel axon growth of a subset of 5-HT neurons. We find that ephrinA5 is required for the exquisite differential targeting of the DR and MnR axons in the olfactory bulb, amygdala and hypothalamus. These observations establish for the first time a role of Eph-ephrinA signaling to organize the broad topography of a monoaminergic system.

## Material and methods

### Animals

Most experiments (gene expression, cell cultures, electroporations) were performed on mice of the Swiss background (RjOrl:SWISS) purchased from a commercial breeder (Centre d'Elevage R. Janvier). E0 was defined as the plug date and P0 as the date of birth.

The Pet1-Cre::RCE-GFP mouse line was used for RT-qPCR analyses. ePet1-Cre mice (Scott et al., 2005) in which the serotonergic specific promoter of the Pet1 gene controls Cre expression were crossed to the RCE-GFP mouse line where enhanced green fluorescent protein is conditionally expressed under the Rosa-26 promoter (Sousa et al., 2009). Pet1-Cre::RCE-GFP mice were bred in our local facility and brains collected from P5, P15 and adult mice.

The ephrinA5-KO mouse line (Frisen et al., 1998) was maintained on a C57Black6 background (Deschamps et al., 2009). Briefly, these mice have a PGK-neo cassette replacing the 5' acceptor splice site and the sequences encoding amino acid residues 42–129. The PCR primers for genotype are as follows: primer 1 (TCCAGCTGTGCAGTTCTCCAAAACA) and primer 2 (ATTCCAGAGGGGTGACTACCACATT) for wild-type sequences (397bp) and primers 1 and primer 3 (AGCCCAGAAAGCGAAGGAGCAAAGC) for mutant sequences (513bp).

All experiments were performed in compliance with the standard ethical guidelines (European Community Guidelines and French Agriculture and Forestry Ministry Guidelines for Handling Animals decree 87849). All efforts were made to reduce the number of animals used and their suffering. Male and female mice were used indiscriminately in all experiments.

## Histology

***Section preparation*** Brains of Swiss mice were collected at embryonic days 12 (E12), E14, E16, E17, E18, at postnatal days 0(P0), P5, P10, P15 and from adult aged over 8 weeks.

Mice aged P5 or younger were anesthetized on ice. Mice older than P5 were anesthetized with pentobarbital, 25mg/kg and xylazine, 5mg/kg. Fixation was either with immersion (E14, E16) or perfusion (>E16) with 4% PFA (4% paraformaldehyde in 0.12M phosphate buffer, pH 7.4). Dissected brains were post-fixed 2 hours (embryonic ages) or overnight (all postnatal ages) before cryoprotection in 10% sucrose and freezing in isopentane cooled with dry ice at -45° to -55°C. In some in situ hybridization (ISH) protocols no post-fixation was performed. Frozen brains were then cut with a cryostat to either coronal or sagittal 20µm thick sections and collected as series of 6. Frozen sections were stored at -80°C before immunohistochemistry or ISH. Some brains were processed as floating sections and sectioned with a freezing microtome. In this case, the brains were cryoprotected in 30% sucrose and frozen directly on the platform of the cryotome at -40°C; serial 40µm thick coronal sections were collected in 1X PBS with 0.01% sodium azide. Sections were stored at 4°C before processing.

***In situ hybridization*** (ISH) was used to analyze EphAs and ephrinAs expression. Digoxigenin-labelled mRNA probes were transcribed from mouse EphA3, EphA4, EphA5, EphA7, and Efna2, Efna3, Efna5, cDNAs. Sense and antisense digest enzymes and polymerases of these probes are listed in Table 1. Sections were air-dried for at least two hours under a hood. Specific antisense RNA probes (0.1-1µg/ml) were mixed with hybridization buffer (50% formamide, 10% dextran sulfate, 1X Denhardt's, 5X SSC and 250 µg/ml tRNA) and incubated at 52°C, 58°C or 65°C for 10mins. 350ul of mixed hybridization buffer was added to each section, covered with a cover-slip, and incubated overnight at the same temperature. The sections were washed with PBS and PBS Triton 0.1% and incubated with anti-Digoxigenin (1/1000) 4° overnight. Sections were washed with 1X PBS and NTMT (Tween 10%; Tris-HCL, pH 9.5, 1M; MgCl2, 1M; NaCl, 5M; H2O) buffer and incubated at 37° with NBT+BCIP or fast red (TR/Naphthol AS-MX Tablets, SIGMA F4523-50 SET) to reveal the reaction. Duration of the revelation (from 2 to 24 hours) was determined empirically according to the sensitivity of the probes and the concentration of the anti-Dig solution. The signal was checked with bright field or fluorescence microscopy. Duration was kept identical for a given experiment (eg. Time course of expression).

The sections were washed with 1X PBS, and mounted in mowiol-Dabco (25 mg/ml) or processed with Immunohistochemistry.

***Immunohistochemistry*** was performed either on alternate series of sections or in combination with ISH. Sections were washed in PBS, then in PGT (PBS with 0.2% gelatin and 0.25% Triton X-100) 4 X 15 mins. Sections were incubated overnight at 4°C with the following primary antibodies: anti-Tph2 (mouse monoclonal, 1/1000, Sigma), anti-5-HT (rabbit polyclonal, 1/1000 Sigma), anti-SERT (rabbit polyclonal, 1/1000, Calbiochem). For fluorescence microscopy, sections were then incubated for 2h at room temperature with the following secondary antibody: donkey anti-rabbit 488 (1/200, Jackson), donkey anti-rabbit Cy3 (1/200, Jackson), donkey anti-mouse 488 (1/200, Jackson), donkey anti-mouse Cy3 (1/200, Jackson), or with phalloidin 594 (1/40 Invitrogen). Then sections were rinsed in PB, mounted in mowiol-Dabco (25 mg/ml) and stored at +4°C.

**RT-qPCR .** Brains of Pet1-Cre::RCE-GFP mice were collected at postnatal day 5, 15 and adult (6 weeks). Brains were kept in 1X PBS on ice and sectioned in the coronal plane with a tissue chopper to 300µm thick sections. The DR was micro dissected under a fluorescent macroscope (Zeiss-MV10) and collected into 5ml tubes, which contained 2ml of cold 1X PBS, a cortical hemisphere was collected as a positive control. To obtain enough tissue for RNA isolation from the raphe, four cases were pooled together for each sample analyzed. Tissue was either directly processed for RNA isolation or fast frozen at -80°C. RNA isolation from tissue was done with Trizol Reagent (Sigma). Samples were weighed (≤ 50mg) before homogenization, PBS was removed extensively and 1ml of trizol was added. Tissue was homogenized and homogenates were transferred to 2ml eppendorf tubes with 0.2ml of chloroform, gently mixed for 15 seconds, and centrifuged 12000g, for 15mins at 4°C. The upper phase was collected and RNA was precipitated with isopropyl alcohol, 0.5ml, incubating at room temperature (5mins), centrifuged at 12000g for 10mins at 4°C. After removal of the supernatant, the RNA pellet was air-dried and dissolved in 100µl Milli-Q water and stored at -80°C.

Possible DNA contamination was cleared using DNase I (Thermo) and RT-PCR was done with the SuperScriptII kit (Invitrogen). Quantitative-PCR was performed with the Thermo SYBR Green Mix kit according to the manufacturers' instruction. Primers are listed in Table 2.

**Raphe culture and collapse assay.** E12 embryos were collected from Swiss timed-pregnant dams. Embryonic hindbrains were rapidly dissected as an 'open book' in ice cold 1X PBS. The rostral and caudal raphe were separated based on anatomical landmarks. The dissected raphe was further cut into 200µm explants with a tissue chopper. Explants were placed onto polylysine/laminin-coated glass coverslips (Marlenfield, 0111540) in 4-well culture boxes (Nunclon, 176740) in DMEM F-12 medium to which BSA (1%), Pen/strep, Glutamine (200mM), Glucose (50%) were added. Explants were cultured for 3-4 days at 37°C, in 5% CO2. For the collapse assay ephrinA5 (R&D System, 374-EA) was added at different concentrations (50mM, 250mM, 500mM) for 1h. Explants were then quickly washed in PBS, fixed in buffered 4% PFA for 30mins, and washed extensively before 5-HT immunocytochemistry (anti-5-HT rabbit polyclonal, 1/1000 from Sigma) and phalloidin 594 (1/40 Invitrogen) staining.

**Quantification of the collapse assay.** Explants were imaged with a fluorescence microscope. Only round-shaped explants which contained 5-HT neurons were quantified, Over 100 growth cones from 3 explants for each condition were counted using a 63X/1.25 objective. The number of collapsed/non collapsed growth cones was counted for both 5-HT axons and non-5-HT axons, comparing the 5-HT immunostaining with the phalloidin staining. Results from 3 independent experiments were used to calculate the mean ratio ± SEM per condition.

**Anterograde Tracing**. We used an adeno-associated virus (AAV1.CAG.tdtomato.WPRE.SV40 ref: AV-1-PV3365, Penn Vector) to express td-tomato fluorescence in the DR neurons and projections. A single injection (20nl of the virus non-diluted) was done in the DR using glass pulled capillaries (5-000-1001-X10, Drummond; puller model 720, KOPF with a heat of 14.5 and solenoid 2). DR stereotaxic injections were performed as previously described (Muzerelle et al., 2016). Adult ephrinA5 KO mice and control littermate (+/+ or +/-) mice were anesthetized with ketamine (150 mg/kg) / xylazine (10 mg/kg). Animals were positioned on a foam board horizontally, the head was fixed and kept horizontal, and Bregma coordinates measured to calculate the position of the injection site and the angle of stereotaxic arm. To target the DR the following coordinates were used: antero-posterior: 0.5mm to lambda; medio-lateral: 1mm; dorsoventral: -3.2mm. The animals were kept for 3 weeks and were perfused by 4% PFA. Brains were processed as described above, collecting serial 50µm coronal sections throughout the brain.

**In utero electroporation of EphrinA construct .** GFP-Efna3 was sub-cloned into the vector pCIG-Td-tomato. The pCIG-Td-tomato vector without the insert was used for the control condition. Both plasmids were purified by Qiagen EndoFree Plasmid Maxi kit, and stored at a final concentration of 2.5µg/µl.

To target gene expression in the amygdala, we followed a previously described in utero electroporation protocol (Remedios et al., 2004; Huang et al., 2014). The plasmids (1µg/µl) were mixed with 1% Fast Green (F7252, Sigma-Aldrich) and injected into one of the lateral ventricles of E12.5 embryos with glass-pulled micropipettes. Then a 3mm diameter electrode (LF650P3, BEX) was placed toward the caudal and ventral part of the telencephalon. Six electric pulses (30V, 50ms pulse length) with 950-ms intervals were applied using an electroporator (CUY21, BEX). After delivery, foster mothers delivering at the same time as the experimental subjects adopted the newborn pups. The electroporated pups were perfused at P5 and processed for immunocytochemistry as described above.

**Image acquisition:** For bright field microscopy, histological sections were imaged using a slide scanner (Nanozoomer 2.0-HT C9600, Hamamatsu, Japan) objective X20 or captured with a Cool SNAP camera mounted on a bright-field microscope (Provis, Olympus,). For illustration purposes, images from the nanozoomer were exported in Tiff format using the NDP View2 software (Hamamatsu, Japan).

For fluorescence microscopy, images were acquired with a Leica DM 6000B system using a 40x/0.70 oil objective (tissue cultures), or acquired on a Leica SP5 confocal system (co-localization and fiber density analyses), equipped with an Argon laser (for the 488nm excitation), a Diode 561nm and HeNe 633nm. Z-stacks of confocal images were acquired at 1024 x 1024 pixel resolution, with a pinhole set to one Airy unit and optimal settings for gain and offset.

**Image analyses *;*** EphA5-Tph2 co-localization was analyzed on P5 brains processed from 3 independent experiments. 20µm-thick cryostat sections through the brainstem were collected as series of 6. One series was processed for combined EphA5 HIS (fast red chromogen), Tph2 immunohistochemistry (revealed with Alexa 488) and DAPI, and imaged with a confocal microscope. These 3 fluorochromes were sequentially acquired with a 40X/1.25 N.A Plan-apochromat objective at 3 different rostrocaudal levels through the raphe (Paxinos Atlas,levels: Bregma -4.3mm, -4.6mm and -4.9mm). The whole hindbrain area containing Tph2+ neurons was acquired including the different subdivisions of

the DR in the dorsal part (DRD), the ventral part (DRV) the lateral wings (DR-LW), and the caudal part (DR-C, B6). Acquisitions included the MnR which comprises the B8 and B5 cell groups, and the supralemniscal B9 cell groups. Confocal stacks were analyzed with image J. A 150µm X 150µm square mask was used for random selection of counting areas. Three random selections were positioned on each distinct 5-HT sub-nucleus. A cell counter plugin was used to count the Tph2 positive cells on individual confocal sections, EphA5 positive cells and the co-localized neurons. It should be noted that in contrast to BCIP the fast red used as a chromogen for ISH mRNA revelation generally diffuses into the nucleus of labelled cells, in contrast to the Tph2 labelling that remains in the cytoplasm (eg. Figure 2 C, Figure 3).

***Fiber density*** was analyzed in two different ways, in cases in anterograde tracer injections and in utero electroporation. In the olfactory bulb and amygdala, confocal images were acquired at 4µm intervals over 20µm in z. A maximum Z-projection of the image stacks was performed with image J. Then, a circular mask of 20µm diameter was used for random sample selection. All labeled fibers that crossed the edge of the mask were counted with a cell counter to compute linear densities. In the hypothalamus, where there is a high density of 5-HT innervation single confocal images were analyzed. Confocal 16 bit images were copied to Image J with an 8-bit format and processed as described (Kiyasova et al. 2011). Subtraction of the background was done with a 20 pixels rollerball and a binary image was obtained after applying a fixed range threshold for all the images. The nuclear region of interest (ROI) was delimited and the area occupied by the labeled fibers was measured within a circular mask (100µm diameter), the mask was randomly placed in 3-5 different locations over the structure, to calculate a mean density value per area and per animal.

**Statistical analyses.** All the statistical analyses applied were performed with GraphPad Prism 6. One-way ANOVA was performed for the Q-PCR, co-localization and collapse assays. To evaluate difference between any of two samples Tukey's multiple comparisons was performed. Student t-test was performed for intergroup comparisons in the fiber density analyses. Unpaired t-test was used for comparison of independent samples and paired t-test was done for analyses comparing, ipsi and contralateral innervation in the same case. Data are expressed as Means +/- SEM, $P<0.05$ was considered as significant.

## Results

### Expression of EphA receptors in the raphe nuclei.

In rodents, 5-HT neurons of the hindbrain start extending axons by embryonic day 12 (E12) reach most of their forebrain targets between E15 and postnatal day 1 (P1) and start arborizing in these targets over the following postnatal days (Lidov and Molliver, 1982 in rats; Kiyasova and Gaspar, 2011, in mice).

We began by screening the expression of the EphA receptors at P5, a time when the 5-HT axons are still actively growing and branching in their targets (Lidov and Molliver, 1982) and where the DR and the MnR can be clearly individualized. Q-PCR analyses were performed on-micro-dissected DR from Pet1-GFP mice (Scott et al., 2005). *EphA3, A4, A5, A6, A7,* and *A8* mRNAs using GAPDH as a housekeeping gene. This analysis showed that *EphA5* is the most abundant EphA receptor in the DR at P5, with lower expression of *EphA4; EphA6, and EphA7*. And no detectable expression of *EphA3* and *EphA8* (Figure 1A). To determine the cellular localization of the *Eph* genes, in situ hybridization (ISH) was performed on consecutive serial coronal sections through the raphe, using specific mRNA probes ot EphAs (Table 1) and to the serotonin transporter (SERT) used as a marked of the 5-HT raphe neurons. This showed that among the Ephs genes examined, only *EphA5* was clearly localized in the DR and the MnR containing 5-HT neurons, but with no visible expression in the raphe magnus, obscurus and pallidus (the B1-3 raphe cell groups)(Figure 1B). The other EphA genes, *EphA4 and EphA7* genes, were not detectable in any of the raphe nuclei but were localized to nuclei, such as the dorsal lateral tegmental nuclei and superior olive, that abut the raphe nuclei (Figure 1B), which likely explains their detection when analyzed by Q-PCR on dissected DR tissue. Sense probes that were used as controls.

Overall, these results indicated a preferential expression of EPhA5 over other EphA receptors in the developing DR and MnR.

### EphA5 expression is dynamically regulated during raphe development

To evaluate the possible developmental impact of EphA5 at different stages of raphe development, we analyzed its expression timeline. Serial sagittal (E14, n=4) and coronal (postnatal and adult) sections were processed for EphA5 ISH P0 (n>5), P5 (n>5), P10 (n>5), P15 (n>5) and adult (n=2). EphA5 expression was detectable in the rostral raphe at E14 (Figure 2 B). This expression was maintained at a high level over the first week following birth and subsequently declined by P15 (Figure 2B) up to adulthood where only weak expression is detectable (not shown). To obtain a quantitative evaluation of the time

course of expression Q-PCR measures of EphA5 mRNA were done on DR tissue from P5, P15 and adult brains (Figure 2A). This showed a significant decrease of EphA5 expression between P5 and P15 ($p<0.05$), consistent with the ISH observation.

These results indicated that EphA5 is dynamically regulated during development with highest expression in early postnatal life with a subsequent decline in expression by P15.

**Serotonergic raphe nuclei differ in EphA5 expression pattern**

Hindbrain raphe nuclei contain a heterogeneous neuronal population that includes in addition to 5-HT neurons, glutamatergic, GABAergic, and peptide-containing neurons. To determine whether EphA5 is specifically expressed in the serotoninergic neurons we combined fluorescent *EphA5* ISH and tryptophan hydroxylase (Tph2) immunocytochemistry (Nguyen et al. 2001) (Figure 2). At E14, 5-HT neurons have not yet achieved their full migration, making it difficult to distinguish clearly all the individual raphe cell groups other than the 2 main rostral and caudal clusters. However a distinction could be made between the dorsal and ventral Tph2+ neurons of the rostral cluster that corresponds to the prospective DR and MnR respectively (Figure 2C). In the dorsal part, a large number of co-localized EphA5-Tph2+ neurons were found (Figure 2C'), whereas rare co-localisation was found in the ventral part. In contrast, in the medulla, the caudal Tph2+ cluster appeared to be entirely segregated from the *EphA5* expressing region.

A more detailed quantitative evaluation of EphA5-Tph2 co-localisation was done at P5, since distinction of these components can be done clearly at this stages (Figure 2 D-E), and this postnatal developmental stage is highly relevant to the ingrowth of 5-HT axons in their targets. Co-localization of Tph2 and was evaluated quantitatively in the different sub-nuclei (Figure 3, tables 3-4). The highest co-localization index was found in the DR (B7- all subcomponents pooled) where more than half of the 5-HT neurons expressed EphA5 (50.2% ± 2.2%, n=3, Figure 3A, D); while the lowest co-localization ratio was noted in the caudal (B1-B3) raphe cell groups (Figure 3C,D). In the MnR (B5, B8), a strong expression of *EphA5* was visible, but only a minority (14-22% respectively) of the 5-HT neurons expressed *EphA5* (Figure 3B, D). Further heterogeneous expression was observed within the DR where co-localization was compared at 3 different rostro-caudal levels (Figure 3E) and in 3 different DR subdivisions (lateral, dorsal, ventral) (Figure 3E and Table 4); Medially located DR neurons have a higher percentage of co-localized neurons than the laterally located DR neurons (Figure 2B, C; Figure 3E). Overall, this co localization pattern indicates a clear topography of EphA5 expression in the raphe subgroups with a rostral to caudal decreasing expression that was visible during embryonic

stages (Figure 2C) and maintained at P5 (Figure 3). Such differences in expression of EhpA5 between the different 5-HT cell groups suggested that EphA5 signaling could be involved in the differential targeting of these various 5-HT neurons.

**Collapse response of 5-HT raphe neurons after the ephrinA application.**

To examine the functional role of EphA5 expression on 5-HT axon outgrowth, we took advantage of the clear-cut differential expression of EphA5 between the rostral (B5-B9) and caudal-medullary (B1-B3) clusters of 5-HT neurons at embryonic ages and compared their response to application of the ligand ephrinA5. Raphe explants from E12 hindbrains, were dissected as illustrated (Figure 4A) and cultured 48h on glass coverslips. In explants from the rostral raphe, ephrinA5-FC induced the collapse of a large fraction of 5-HT growth cones (Figure 4-B). A dose dependent effect was noted: 71.3% ± 4.5% of the 5-HT growth cones were collapsed at the highest concentration tested (500ng/ml) and 45-50% at intermediate concentrations (50-250ng/ml) (Figure 4C). In caudal raphe explants, ephrinA5 application did not induce a significant collapse response compared to controls at any of the concentrations tested (Figure 4 B2, 4D).

Because EphA5 is also expressed in a large number of non-5HT neurons in both the rostral and caudal raphe areas (table 3), we also measured the collapse responses of the non-5-HT axons. The non-5-HT growth cones showed a significant dose-dependent collapse response in both rostral and caudal explants (Figure 4 E, F), thus not displaying the regional selectivity noted for 5-HT growth cones.

Overall, these experiments demonstrated that the pattern of EphA5 expression in 5-HT raphe neurons correlated with a repulsive response to the application of ephrinA5-FC. Interestingly, there was a dose response effect suggesting that differences in the ligand/receptor ratio could contribute to a differential targeting of 5-HT raphe neurons.

**5-HT innervation is reduced by ectopic ephrinA expression in the amygdala.**

Next, we investigated the effects of ephrinA ligands for *in vivo* 5-HT axon targeting using an over-expression strategy. We focused on the amygdala and piriform cortex which are preferential targets of the DR 5-HT neurons (Muzerelle et al. 2016), and express only very low levels of the main EphA5 ligands, ephrinA2, ephrinA3 and ephrinA5, based on our own observations, confirming previously published reports (Deschamps et al., 2010, Gerstmann et al. 2015) and available public resources (Allen Brain Atlas, http://developingmouse.brain-map.org/gene/show/13415, 13416, 13418). This suggested that the amygdala and piriform cortex could be permissive for the ingrowth of DR axons

which express high level of EphA5 receptors. To examine this possibility, we used an in utero electroporation strategy to ectopically express ephrinA3 that has been shown to have the highest affinity for EphA5 (Gale et al. 1996). An ephrinA3 cDNA fragment was sub-cloned into a pCIG-Tdtomato vector; the plasmid with or without the ephrinA3 insert was electroporated into the amygdala and piriform cortex at E12.5 and the brains processed at P5 for 5-HT immunocytochemistry. Not structural changes were observed on the electroporated/non electroporated side, as evaluated by Nissl staining. The electroporated cells were visible in different parts of the amygdala (basolateral and basomedial amygdaloid nucleus), and in the piriform cortex (Figure 5A, B, C). Measures of 5-HT fiber density showed a significant decrease of 5-HT fibers on the electroporated amygdala (0.07±0.01 fibers/µm) and piriform cortex (0.07±0.01 fibers/µm) compared to the contralateral non-electroporated amygdala (0.21±0.03 fibers/µm) and piriform cortex (Figure 5D, 7E,). Conversely, in the cases electroporated with the control vector, the density of 5-HT fibers was unchanged compared to the non-electroporated side. This result indicated that ectopic expression of ephrinA3 during development can specifically reduce the 5-HT raphe-amygdala innervation ($n=5$, $p < 0.005$).

**EphrinA5 is required for the differential forebrain targeting of B7/B8 raphe neurons**

To investigate the role of endogenous ephrins in 5-HT axon targeting, we investigated the effects of loss of function of one of the major EphA5 ligands, ephrinA5. Using the ephrinA5 KO mouse model. We reasoned that 5-HT neurons with high EphA5 expression in the raphe should avoid innervating brain regions containing high levels of the ligand ephrinA5. ISH of an Efna5 riboprobe was done on serial sections of P5 brains. We focused on 3 main regions with high ephrinA5 expression, namely the olfactory bulb (OB) (Fig 6C), the ventromedial hypothalamus (VMH) and the suprachiasmatic nucleus (SCN) (Figure 7 A, F). Indeed, previous selective anterograde tracing from these DR and MnR had shown that the DR targets the granule cell layer of the OB and seems arrested by the mitral cell layer, whereas the MnR targets the glomerular layer (GL) of the OB (Figure 6C) (Steinfeld 2015, Muzerelle et al., 2016). Similarly, 5-HT DR axons consistently avoid the VMH and SCN that are instead innervated by MnR raphe neurons (Bang et al. 2012, Muzerelle et al. 2016)

Anterograde tracing of the DR neurons was done with an AAV viral vector expressing Td-tomato comparing ephrinA5 KO and WT mice. We evaluated the extent of anterogradely labeled neurons that are 5-HT-immunopositive in the raphe (Figure 6A) and the

size of the injection site (Figure 6B). Transfection was limited to the DR (Figure 6B) and the number of transfected 5-HT cells was equivalent in the control and mutant mice. Anterogradely labeled axons were further characterized as serotonergic (or not), using 5-HT transporter (SERT) immunohistochemistry (Figure 6 D', E').

In the OB of WT mice, anterogradely labeled axons, all of which were SERT+, were restricted to the granular cell layer (GCL) and appeared to be arrested at the edge of the mitral cell layer (ML) that expresses high ephrinA5 levels (Figure 6C); only a few fibers entering into the external plexiform layer (EPL) (Figure 6D-D'), confirming previous observations (Steinfeld et al. 2015, Muzerelle et al. 2016). In the ephrinA5 KO mice, DR axons did not seem to be arrested by the ML, which they crossed, arborizing into the EPL (Figure 6E-E'). To obtain quantitative measures normalized to the number of anterogradely labeled axons, we estimated the density of td tomato labeled fibers in the CGL and the EPL, and calculated the EPL/CGL ratio. This ratio was significantly increased in ephrinA5 KO mice compared to WT mice (Figure 6F). To determine whether the overall density of 5-HT labeled axons was modified, we measured the density of SERT-labeled axons in the CGL and the EPL and found an overall increase in the density of 5-HT axons in the EPL but not in the CGL (Figure 6 G, H). This indicates that the increased EPL/CGL ratio in ephrinA5 KO mice is not the consequence of a general increase in the number of 5-HT axons reaching the OB, but rather due to an increase in the fraction of DR axons that cross beyond the ML.

In the same cases, we further analyzed DR anterograde labeling and global 5-HT innervation in two hypothalamic areas that show high ephrinA5 expression: the ventromedial hypothalamus (VMH) (Figure 7A) and the suprachiasmatic nucleus (SCN) (Figure 7F). Both nuclei show a high level of ephrinA5 at P5 (Figure 7A, F). In WT mice, anterograde labeling from the DR shows that both the VMH and the SCN are not targeted by DR axons (Figure 7B', G') confirming previous observations (Bang et al. 2012, Muzerelle et al., 2016). However, these areas contain a very high density of SERT+ labeled terminals that originate mainly from the MnR. In the ephrinA5 KO mice, the density of DR anterograde projection was substantially increased in both the VMH (Figure 7C', E) and the SCN (Figure 7H', J). Double labeling (td-tomato and SERT) showed that both 5-HT and non 5-HT DR axons contributed to this increase (Figure 7C", H"). However the overall density of SERT+ labeled fibers also showed a significant increase in the VMH (Figure 7E,I).

These experiments indicated a requirement of ephrinA5 for the targeting of the DR axons, showing that the absence of ephrinA5 results in an increased serotoninergic innervation of distinctive layers of the OB and of key hypothalamic nuclei resulting in an overall increase of the 5-HT innervation in these areas (Figure 8).

## Discussion

Our results demonstrate for the first time a role of ephrinA signaling for the selective targeting of serotoninergic raphe nuclei. We show that EphA5 is differentially expressed across the different hindbrain raphe nuclei, and that this correlates with a different repulsive action of ephrinA on 5-HT axon growth. Ectopic expression of ephrinA inhibits the ingrowth of 5-HT raphe axons in main targets of the dorsal raphe 5-HT neurons and ephrinA5 loss of function causes a mis-targeting of dorsal raphe 5-HT axons resulting in localized increases in 5-HT innervation.

The development of raphe neurons has been well outlined by classical morphological studies in rodents (Lidov and Molliver, 1982; Wallace and Lauder, 1983), however, only few insights have been obtained to date into the molecular control of axon guidance in this system. Wnt signals have been implicated in the polarity of 5-HT neurons (Fenstermaker et al., 2010) and Slit/Robo signaling influences 5-HT axon tract organization in the medial forebrain bundle (Bagri et al., 2002), but hardly anything is known about the molecular control of selective 5-HT axon targeting. This knowledge gap is likely due to a prevailing view of 5-HT neurons as a diffuse highly collateralized system with limited specificity (Agnati et al., 2006). However, increasing evidence showed that raphe 5-HT neurons are in fact heterogeneous in their molecular identities (Wylie et al., 2010; Fernandez et al., 2015; Okaty et al., 2015), their physiology (Calizo et al., 2011; Fernandez and Gaspar, 2012) , their genetic determinants (Kiyasova et al., 2011), and their connectivity (Azmitia and Segal, 1978; Commons, 2015; Muzerelle et al., 2016). In addition to the established divergence of axons arising from the rostral and caudal 5-HT neuron clusters (directed toward the forebrain and the spinal cord respectively), there is a distinct topographic organization within the ascending forebrain projections. 5-HT axons originating from the DR and MnR occupy complementary terminal territories in the forebrain (Bobillier et al., 1976; Azmitia and Segal, 1978; Jacobs et al., 1978; Vertes et al., 1999; Muzerelle et al., 2016). Coinciding with this topographic anatomical organization, our study revealed a gradient of EphA5 gene expression with higher EphA expression in the DR than in the MnR, and in addition a clear rostral to caudal and medial to lateral ex-

pression gradient. Thus, high EphA5 expression in DR neuronal subsets could explain why DR 5-HT neurons do not innervate brain areas that have high expression of ephrinA, which are instead innervated by 5-HT neurons from the MnR. This is particularly clear in the case of the olfactory bulb (OB), where DR and MnR 5-HT neurons are located respectively in the central (GCL) or outer (EPL, GL) layers of the OB (Steinfeld et al 2015; Muzerelle et al., 2016). The ephrinA3/5 expressing mitral cell layer might then act as a barrier to prevent DR 5-HT axons from crossing into the outer OB layers. Similarly, hypothalamic nuclei that normally receive all (suprachiasmatic) or a majority (VMH) of their 5-HT innervation from the MnR (Bang et al., 2012; Muzerelle et al., 2016) show high levels of ephrinA expresion during development. The implication of ephrinA was supported by altered distribution of DR axons. In both the OB and the hypothalamus, 5-HT innervation was increased and anterogradely labeled axons from the DR were misplaced as though an inhibitory barrier was removed. Conversely, when an ephrinA ligand was ectopically expressed in a structure such as the amygdala, which is a preferential target of the DR 5-HT innervation (Muzerelle et al., 2016), the ingrowth of 5-HT raphe axons was significantly reduced. Thus, present results indicate that ephrinA5 signaling contributes to the selective targeting of 5-HT axons in the forebrain by repelling the ingrowth of 5-HT axons originating from the DR, in brain regions that are normally targeted by the MnR.

EphrinA signaling may also influence other aspects of the topography of DR; this is suggested by our observation of a difference of EphA5 expression in the medial lateral parts of the DR which coincides with differential anatomical projections. 5-HT neurons in the lateral wings of the DR have a low level of EphA expression and project to regions with high ephrinA5 expression such as the lateral geniculate nucleus (Muzerelle et al. 2016, Wilks et al. 2010). It will be interesting to determine in the future how the combination of axon guidance molecules in raphe targets contribute to attracting subsets of 5-HT axons to defined brain areas/layers. In particular we do not know what factors attract the MnR 5-HT axons to the areas that are avoided by the DR. Intriguingly 5-HT itself could contribute to this growth-promoting effects, since a defective innervation of the SCN was observed in Tph2-KO mice (Migliarini et al., 2013). The mis-targeting of DR axons in the hypothalamus of ephrinA5 KO mice concerned both 5-HT and non 5-HT neurons of the DR, indeed as noted in the present study, both cell types express EphA5. These common axon guidance cues are consistent with shared connectivity profiles; indeed, previous anatomical tracing studies showed that DR afferents frequently contain a mix of 5-HT

and non 5-HT neurons (Steinbusch and Nieuwenhuys, 1981; Kiyasova et al., 2011), the latter could include glutamatergic Vglut3+ (Hioki et al., 2010) and GABAergic neurons (Bang et al., 2012). Thus DR neurons could share similar axon guidance mechanisms, independent of their neurotransmitter content.

EphA-ephrinA signaling is involved in several neuronal developmental processes from cell migration to synaptic maturation (rev. in Cramer and Miko, 2016; Kania and Klein, 2016) although its best known implication in neural development is for axon guidance, where both repulsive and attractive interactions have been described. Our current studies indicated a main inhibitory effect of the ephrinA ligands on 5-HT axon growth: *in vitro,* ephrinA5 induced a collapse of the growth cones and *in vivo* ectopic expression of ephrinA3 inhibited 5-HT axon ingrowth. This corresponds to the classic repulsive forward signaling of EphA receptor activation (Kania and Klein, 2016), and is most likely due to the EphA5 receptor according to the present localization studies. However we cannot exclude the implication of other EphAs since transcriptional profiling of raphe neurons in embryonic and postnatal brains reported also the presence of other EphA (Wylie et al., 2010; Okaty et al., 2015), but likely expression is at levels that are too low for our ISH detection. Moreover, the loose specificity of the EphA5 receptors for ephrinA ligands and the redundancy of ephrinA expression in several brain targets (such as the mitral cells in the OB) suggest that the defects of 5-HT axon targeting observed in the ephrinA5 KO might be more pronounced in double or triple ephrinA KO mice. Such redundancy has previously been observed in the visual system (Feldheim et al., 2000).

In the visual and auditory sensory maps Eph-ephrinA signaling acts to build a continuous topographic map (Cramer and Miko, 2016) however present results do not indicate that this is the case in the 5-HT raphe system where topography is much looser. Indeed DR and MnR have different targets but do not display further topographic organization within their prefered targets. Thus, we propose that as regards the 5-HT systems, Eph-ephrinA signaling could act in a target selection process, by generating non permissive boundaries for the ingrowth of DR 5-HT raphe subtypes. This effect would then be more similar of that observed for the motor neurons when choosing a dorsal/ventral muscle targets during development (Eberhart et al., 2004).

EphA5 expression in 5-HT raphe neurons was dynamically expressed, being maximal during axon growth in embryonic life and target reaching during the early postnatal

559 period and showing decreased expression, similarly to what has reported for ephrinA5
560 expression (Deschamps et al., 2010). Given the potential of 5-HT neurons to regenerate
561 and grow, it will be interesting to know whether the present developmental mechanisms
562 are reactivated after a lesion, and whether the propensity of serotonin axons to regrow
563 (Mullner et al., 2008) could be linked to their EphA content.

564 What could be the pathophysiological consequences of targeting defects of raphe
565 neurons in the olfactory bulb or the hypothalamus? Our observations in ephrinA5 KO
566 showed that mis-targeting of the DR axons was correlated with a general increase of 5-
567 HT innervation in these regions, suggesting that excitatory/inhibitory balance is compro-
568 mised in these brain nuclei. Interestingly, behavioral observations conducted in the
569 ephrinA5 and EphA5 KO mice showed some common phenotypes that could relate to
570 our observations. Both studies report a reduction in inter-male aggression (Mamiya et al.,
571 2008; Sheleg et al., 2015) and increase of 5-HT levels in the hypothalamus was shown in
572 the EphA5 KO (Mamiya et al., 2008) consistent with our observations of increased 5-HT
573 innervation in this brain region. Interestingly the increased 5-HT innervation that we ob-
574 served in the ephrinA5 KO was concentrated in the ventrolateral part (VMHVL), which
575 has been specifically implicated in modulating aggression (Martinez et al 2008; Silva et
576 al. 2016). Clearly, the possible pathophysiological consequences of SCN hyper-
577 innervation calls for further studies on the circadian rhythms of these mutants, given the
578 implication of 5-HT innervation to the SCN in entraining circadian rhythmicity (Versteeg et
579 al., 2015)

580 Given the implication of 5-HT in a wide range of behaviors, and psychiatric disorders, our
581 study point to new gene targets that may indirectly affect 5-HT functions by changing the
582 targeting of raphe neurons and inducing modifications of 5-HT inputs in selected brain
583 regions.

584 **References**

585 Agnati LF, Leo G, Zanardi A, Genedani S, Rivera A, Fuxe K, Guidolin D (2006) Volume
586 transmission and wiring transmission from cellular to molecular networks: history
587 and perspectives. Acta physiologica (Oxford, England) 187:329-344.
588 Azmitia EC, Segal M (1978) An autoradiographic analysis of the differential ascending
589 projections of the dorsal and median raphe nuclei in the rat. The Journal of com-
590 parative neurology 179:641-667.
591 Bagri A, Marin O, Plump AS, Mak J, Pleasure SJ, Rubenstein JL, Tessier-Lavigne M
592 (2002) Slit proteins prevent midline crossing and determine the dorsoventral posi-
593 tion of major axonal pathways in the mammalian forebrain. Neuron 33:233-248.
594 Bang SJ, Jensen P, Dymecki SM, Commons KG (2012) Projections and interconnections
595 of genetically defined serotonin neurons in mice. The European journal of neuro-
596 science 35:85-96.
597 Bobillier P, Seguin S, Petitjean F, Salvert D, Touret M, Jouvet M (1976) The raphe nuclei
598 of the cat brain stem: a topographical atlas of their efferent projections as revealed
599 by autoradiography. Brain research 113:449-486.
600 Brust RD, Corcoran AE, Richerson GB, Nattie E, Dymecki SM (2014) Functional and de-
601 velopmental identification of a molecular subtype of brain serotonergic neuron
602 specialized to regulate breathing dynamics. Cell reports 9:2152-2165.
603 Calizo LH, Akanwa A, Ma X, Pan YZ, Lemos JC, Craige C, Heemstra LA, Beck SG
604 (2011) Raphe serotonin neurons are not homogenous: electrophysiological, mor-
605 phological and neurochemical evidence. Neuropharmacology 61:524-543.
606 Commons KG (2015) Two major network domains in the dorsal raphe nucleus. The Jour-
607 nal of comparative neurology 523:1488-1504.
608 Cooper MA, Kobayashi K, Zhou R (2009) Ephrin-A5 regulates the formation of the as-
609 cending midbrain dopaminergic pathways. Developmental neurobiology 69:36-46.
610 Cramer KS, Miko IJ (2016) Eph-ephrin signaling in nervous system development.
611 F1000Research 5.
612 Crawford LK, Craige CP, Beck SG (2010) Increased intrinsic excitability of lateral wing
613 serotonin neurons of the dorsal raphe: a mechanism for selective activation in
614 stress circuits. Journal of neurophysiology 103:2652-2663.
615 Deakin JF, Graeff FG (1991) 5-HT and mechanisms of defence. Journal of psychophar-
616 macology (Oxford, England) 5:305-315.

617 Deschamps C, Faideau M, Jaber M, Gaillard A, Prestoz L (2009) Expression of ephrinA5
618 during development and potential involvement in the guidance of the mesostriatal
619 pathway. Experimental neurology 219:466-480.
620 Deschamps C, Morel M, Janet T, Page G, Jaber M, Gaillard A, Prestoz L (2010) EphrinA5
621 protein distribution in the developing mouse brain. BMC neuroscience 11:105.
622 Eberhart J, Barr J, O'Connell S, Flagg A, Swartz ME, Cramer KS, Tosney KW, Pasquale
623 EB, Krull CE (2004) Ephrin-A5 exerts positive or inhibitory effects on distinct sub-
624 sets of EphA4-positive motor neurons. The Journal of neuroscience 24:1070-1078.
625 Feldheim DA, Kim YI, Bergemann AD, Frisen J, Barbacid M, Flanagan JG (2000) Genetic
626 analysis of ephrin-A2 and ephrin-A5 shows their requirement in multiple aspects of
627 retinocollicular mapping. Neuron 25:563-574.
628 Fenstermaker AG, Prasad AA, Bechara A, Adolfs Y, Tissir F, Goffinet A, Zou Y, Paster-
629 kamp RJ (2010) Wnt/planar cell polarity signaling controls the anterior-posterior
630 organization of monoaminergic axons in the brainstem. The Journal of neurosci-
631 ence : the official journal of the Society for Neuroscience 30:16053-16064.
632 Fernandez SP, Gaspar P (2012) Investigating anxiety and depressive-like phenotypes in
633 genetic mouse models of serotonin depletion. Neuropharmacology 62:144-154.
634 Fernandez SP, Cauli B, Cabezas C, Muzerelle A, Poncer JC, Gaspar P (2016) Multiscale
635 single-cell analysis reveals unique phenotypes of raphe 5-HT neurons projecting
636 to the forebrain. Brain structure & function. 221:4007-4025.
637 Frisen J, Yates PA, McLaughlin T, Friedman GC, O'Leary DD, Barbacid M (1998) Ephrin-
638 A5 (AL-1/RAGS) is essential for proper retinal axon guidance and topographic
639 mapping in the mammalian visual system. Neuron 20:235-243.
640 Gerstmann K, Pensold D, Symmank J, Khundadze M, Hübner CA, Bolz J, Zimmer
641 G.(2015)Thalamic afferents influence cortical progenitors via ephrin A5-EphA4 in-
642 teractions. Development. 142:140-50.
643 Hale MW, Lowry CA (2011) Functional topography of midbrain and pontine serotonergic
644 systems: implications for synaptic regulation of serotonergic circuits. Psychophar-
645 macology 213:243-264.
646 Hioki H, Nakamura H, Ma YF, Konno M, Hayakawa T, Nakamura KC, Fujiyama F, Kaneko
647 T (2010) Vesicular glutamate transporter 3-expressing nonserotonergic projection
648 neurons constitute a subregion in the rat midbrain raphe nuclei. The Journal of
649 comparative neurology 518:668-686.

650 Huang TN, Chuang HC, Chou WH, Chen CY, Wang HF, Chou SJ, Hsueh YP (2014) Tbr1
651 haploinsufficiency impairs amygdalar axonal projections and results in cognitive
652 abnormality. Nature neuroscience 17:240-247.
653 Imai H, Matsukawa M, Okado N (2004) Lamina-selective changes in the density of syn-
654 apses following perturbation of monoamines and acetylcholine in the rat medial
655 prefrontal cortex. Brain research 1012:138-145.
656 Jacobs BL, Azmitia EC (1992) Structure and function of the brain serotonin system. Phys-
657 iological reviews 72:165-229.
658 Jacobs BL, Foote SL, Bloom FE (1978) Differential projections of neurons within the dor-
659 sal raphe nucleus of the rat: a horseradish peroxidase (HRP) study. Brain research
660 147:149-153.
661 Jensen P, Farago AF, Awatramani RB, Scott MM, Deneris ES, Dymecki SM (2008) Rede-
662 fining the serotonergic system by genetic lineage. Nature neuroscience 11:417-
663 419.
664 Kania A, Klein R (2016) Mechanisms of ephrin-Eph signalling in development, physiology
665 and disease. Nature reviews Molecular cell biology 17:240-256.
666 Kiyasova V, Gaspar P (2011) Development of raphe serotonin neurons from specification
667 to guidance. The European journal of neuroscience 34:1553-1562.
668 Kiyasova V, Fernandez SP, Laine J, Stankovski L, Muzerelle A, Doly S, Gaspar P (2011)
669 A genetically defined morphologically and functionally unique subset of 5-HT neu-
670 rons in the mouse raphe nuclei. The Journal of neuroscience : the official journal of
671 the Society for Neuroscience 31:2756-2768.
672 Lidov HG, Molliver ME (1982) Immunohistochemical study of the development of sero-
673 tonergic neurons in the rat CNS. Brain research bulletin 9:559-604.
674 Lucki I (1998) The spectrum of behaviors influenced by serotonin. Biological psychiatry
675 44:151-162.
676 Mamiya PC, Hennesy Z, Zhou R, Wagner GC (2008) Changes in attack behavior and
677 activity in EphA5 knockout mice. Brain research 1205:91-99.
678 Martinez, R.C.R., Carvalho-Netto, E.F., Amaral, V.C.S., Nunes-de-Souza,R.L. & Canteras,
679 N.S. (2008) Investigation of the hypothalamic defensive system in the mouse. Behav.
680 Brain Res., 192, 185–190.
681
682

683 Migliarini S, Pacini G, Pelosi B, Lunardi G, Pasqualetti M (2013) Lack of brain serotonin
684 affects postnatal development and serotonergic neuronal circuitry formation. Mo-
685 lecular psychiatry 18:1106-1118.
686 Miko IJ, Nakamura PA, Henkemeyer M, Cramer KS (2007) Auditory brainstem neural ac-
687 tivation patterns are altered in EphA4- and ephrin-B2-deficient mice. The Journal
688 of comparative neurology 505:669-681.
689 Mullner A, Gonzenbach RR, Weinmann O, Schnell L, Liebscher T, Schwab ME (2008)
690 Lamina-specific restoration of serotonergic projections after Nogo-A antibody
691 treatment of spinal cord injury in rats. The European journal of neuroscience
692 27:326-333.
693 Muzerelle A, Scotto-Lomassese S, Bernard JF, Soiza-Reilly M, Gaspar P (2016) Condi-
694 tional anterograde tracing reveals distinct targeting of individual serotonin cell
695 groups (B5-B9) to the forebrain and brainstem. Brain structure & function 221:535-
696 561.
697 Nguyen, T., Chin, W. C., O'Brien, J. A., Verdugo, P., & Berger, A. J. (2001). Intracellular
698 pathways regulating ciliary beating of rat brain ependymal cells. J Physiol, 531(Pt
699 1), 131-140.
700 O'Leary DD, Wilkinson DG (1999) Eph receptors and ephrins in neural development.
701 Current opinion in neurobiology 9:65-73.
702 Okaty BW, Freret ME, Rood BD, Brust RD, Hennessy ML, deBairos D, Kim JC, Cook
703 MN, Dymecki SM (2015) Multi-Scale Molecular Deconstruction of the Serotonin
704 Neuron System. Neuron 88:774-791.
705 Pflieger JF, Clarac F, Vinay L (2002) Postural modifications and neuronal excitability
706 changes induced by a short-term serotonin depletion during neonatal development
707 in the rat. The Journal of neuroscience : the official journal of the Society for Neu-
708 roscience 22:5108-5117.
709 Prakash N, Vanderhaeghen P, Cohen-Cory S, Frisen J, Flanagan JG, Frostig RD (2000)
710 Malformation of the functional organization of somatosensory cortex in adult
711 ephrin-A5 knock-out mice revealed by in vivo functional imaging. The Journal of
712 neuroscience : the official journal of the Society for Neuroscience 20:5841-5847.
713 Prestoz L, Jaber M, Gaillard A (2012) Dopaminergic axon guidance: which makes what?
714 Frontiers in cellular neuroscience 6:32.

Remedios R, Subramanian L, Tole S (2004) LIM genes parcellate the embryonic amygdala and regulate its development. The Journal of neuroscience : the official journal of the Society for Neuroscience 24:6986-6990.

Schmidt BJ, Jordan LM (2000) The role of serotonin in reflex modulation and locomotor rhythm production in the mammalian spinal cord. Brain research bulletin 53:689-710.

Scott MM, Wylie CJ, Lerch JK, Murphy R, Lobur K, Herlitze S, Jiang W, Conlon RA, Strowbridge BW, Deneris ES (2005) A genetic approach to access serotonin neurons for in vivo and in vitro studies. Proceedings of the National Academy of Sciences of the United States of America 102:16472-16477.

Sheleg M, Yochum CL, Richardson JR, Wagner GC, Zhou R (2015) Ephrin-A5 regulates inter-male aggression in mice. Behavioural brain research 286:300-307.

Sousa VH, Miyoshi G, Hjerling-Leffler J, Karayannis T, Fishell G (2009) Characterization of Nkx6-2-derived neocortical interneuron lineages. Cerebral cortex (New York, NY : 1991) 19 Suppl 1:i1-10.

Silva BA, Mattucci C, Krzywkowski P, Cuozzo R, Carbonari L, Gross CT. (2016) The ventromedial hypothalamus mediates predator fear memory. Eur J Neurosci., 43:1431-9.

Steinbusch HW, Nieuwenhuys R (1981) Localization of serotonin-like immunoreactivity in the central nervous system and pituitary of the rat, with special references to the innervation of the hypothalamus. Advances in experimental medicine and biology 133:7-35.

Steinfeld R, Herb JT, Sprengel R, Schaefer AT, Fukunaga I. (2015) Divergent innervation of the olfactory bulb by distinct raphe nuclei. J Comp Neurol, 523:805-13.

Teissier A, Chemiakine A, Inbar B, Bagchi S, Ray RS, Palmiter RD, Dymecki SM, Moore H, Ansorge MS (2015) Activity of Raphe Serotonergic Neurons Controls Emotional Behaviors. Cell reports 13:1965-1976.

Trowbridge S, Narboux-Nême N, Gaspar P. (2011) Genetic Models of Serotonin (5-HT) depletion: what do they tell us about the developmental role of 5-HT? *Anat Rec(Hoboken)*. 294:1615-23

Versteeg RI, Serlie MJ, Kalsbeek A, la Fleur SE (2015) Serotonin, a possible intermediate between disturbed circadian rhythms and metabolic disease. Neuroscience 301:155-167.

Vertes RP, Fortin WJ, Crane AM (1999) Projections of the median raphe nucleus in the rat. The Journal of comparative neurology 407:555-582.

749 Wallace JA, Lauder JM (1983) Development of the serotonergic system in the rat em-
750 bryo: an immunocytochemical study. Brain research bulletin 10:459-479.
751 Wilks TA, Rodger J, Harvey AR (2010) A role for ephrin-As in maintaining topographic
752 organization in register across interconnected central visual pathways. The Euro-
753 pean journal of neuroscience 31:613-622.
754 Wylie CJ, Hendricks TJ, Zhang B, Wang L, Lu P, Leahy P, Fox S, Maeno H, Deneris ES
755 (2010) Distinct transcriptomes define rostral and caudal serotonin neurons. The
756 Journal of neuroscience : the official journal of the Society for Neuroscience
757 30:670-684.
758
759
760

761 **Figure Legends**

762 **Figure 1 - EphA receptor gene expression in the developing mouse raphe.**

763 A, Q-PCR of EphA3, EphA4, EphA5, EphA6, EphA7 and EphA8 mRNAs in DR extracts
764 from P5 mice (n=4 mice /experiment) Relative mRNA expression was calculated as $2^{-\Delta Ct}$
765 (delta of cycle threshold) Data are presented as mean ± SEM from 3 independent ex-
766 periments.

767 B, In situ hybridization of SERT, EphA3, EphA4, EphA5 and EphA7 mRNAs is shown at 3
768 different rostro-caudal levels of the raphe nuclei, including the DR (B7), the caudal DR
769 (B6), the rostral MnR (B8), the caudal MnR (B5), the raphe pallidus (B1), obscurus (B2),
770 and magnus (B3). Coronal serial sections (20µm thick) were labeled with the 5 different
771 probes. The localization of the 5-HT neurons as revealed by SERT expression was out-
772 lined with dashed yellow lines that were transferred to the consecutive sections on the
773 series. This shows that only EphA5 labeling coincides clearly with the contours of B7
774 and B8. EphA4 and EphA7 are also strongly expressed in the brainstem but signal is
775 mainly detected in cell groups such as the dorsal anterior tegmental nucleus (atg) or the
776 dorsal tegmental nucleus (dtg) or the inferior olive (io) that come very close to the raphe.
777 Scale bar= 250µm

778 **Figure 2- EphA5 is expressed in serotonergic neurons during embryonic and post-**
779 **natal development.**

780 A- Q-PCR of EphA5 mRNAs in DR extracts from P5 (n=3), P15 (n=3) and adult (n=3).
781 Relative mRNA expression was calculated as $2^{-\Delta Ct}$. Data are presented as mean ± SEM
782 from 3 independent experiments,

783 B- Time course of EphA5 expression in the developing raphe was analyzed on sagittal
784 (E14) and coronal (P0, P5, P10, P15) sections through the raphe nuclei. Note the de-
785 crease in EphA5 expression by P15. No expression is detected using the sense probe of
786 EphA5, Scale bar=500µm.

787 C- Co-localization was visualized on confocal images after Tph2-immunostaining (green)
788 and EphA5 ISH (red). Sagittal section of E14 mouse brain through the rostral (R) and
789 caudal (C) raphe clusters that are indicated with arrows. Note that the dorsal part of the
790 rostral cluster overlaps with EphA5 labeling, whereas the ventral part does not. C',
791 shows a higher power image of the boxed area in 2A. Arrows indicate co-localized neu-
792 rons (red nuclear labeling for EphA5 and green cytoplasmic labeling for Tph2); the as-

terisk shows Tph2 + neurons with no EphA5 expression. Scale bar=1 mm (A), 100 µm (A')

D, E, F, Coronal sections of a P5 mouse hindbrain at 3 a rostral (B), intermediate (C) and caudal (C) levels of the raphe. Sections were counter-stained with DAPI. Scale bar=500 µm

**Figure 3- Quantification of EphA5-Tph2 co-localization in distinct raphe nucleus.**

A-C, High power confocal images in B7, B8 and B2, showing the difference in co-localization of EphA5 and Tph2 in different raphe nuclei. White arrows point to Tph2+EphA5 co-localized neurons whereas the arrowheads show neuron containing only EphA5. Scale bar=50µm

D, E, Histograms summarizing the % co-localization among the different raphe nuclei, subdivided as the B1-B9 cell groups (D) and within the DR where co-localization was compared at 3 different rostro-caudal levels : caudal DR DR-C), middle DR (DR-M ), rostral DR (DR-R) and in 3 different DR subdivisions: DR lateral (DR-L), DR-dorsal (DR-D), and DR ventral (DR-V). Data are presented as mean ± SEM (n=3), one-way Anova, ***p<0.005 and ****p<0.001.

**Figure 4- EphrinA5 induces collapse of rostral raphe serotonin axons in vitro.**

A, Explant preparation: hindbrain was dissected as an 'open book' from E12 embryos; the rostral and caudal raphe were dissected as depicted on a whole mount E12 hind-brain stained for 5-HT. Scale bar=2mm.

B; Raphe explants (3DIV) were stained for 5-HT (green) and phalloidin (red). B1- shows the 5-HT+ axons emerging from the explant; B2-5 shows 5-HT-labelled growth cones displaying either a normal fan-like morphology (B2, B3) or collapsed growth cone that have branch-like morphology (B4) or a long trailing process and an actin rich retraction bulb . Scale bar=100µm (B1), 10µm (B2-B5)

C, D, E, F, Histograms show the % of collapsed growth cones when explants are ex-posed to different concentrations of ephrinA5. C-D) 5-HT-labeled axons from rostral (C) and caudal (D) explants; E-F) non-5-HT axons from rostral (E) and caudal (F) explants. (> 5 explants and >100 growth cones per condition). Data are presented as mean ± SEM, one-way anova, *p<0.05, **p<0.01, ***p<0.005 and ****p<0.001.

**Figure 5- Overexpression of ephrinA3 down regulates serotonergic innervation in**

**the amygdala and piriform cortex.**

A-A", B-B", Electroporated neurons were revealed by td-tomato with the ephrinA3 plasmid in the targets of Am (A) and Pir (B). Corresponding 5-HT immunocytochemistry from the electroporated (A', A') and non electroporated (A", A") sides. Note the decrease of 5-HT fibers in the outlined area compared to the control side. Scale bar=100µm

C, Target of electroporation (td-tomato) on a coronal section of P5 mouse brain at the level of amygdala. Arrows show electroporated Am and Pir. Scale bar=1000µm

D, E, Scatterogram shows serotonergic fiber density in the electroporated (red) versus non electroporated (blue) amygdala (D) and piriform cortex (E). Overexpression of ephrinA3 resulted in a significant decrease of 5-HT fiber density compared to the control groups, (n=5). Data are presented as mean ± SEM, paired t test was used for ipsi vs. contra, ***p<0.005.

**Figure 6- Anterograde tracing from dorsal raphe to olfactory bulb in ephrinA5-/- mice.**

A, AAV-tdtomato virus was injected in the DR. Injection sites were checked with 5-HT immunohistochemistry on the coronal raphe sections, showing 5-HT and td-tomato labeling in the DR but not in the MnR (A). Scale bar=500µm (A left), 50µm (A right)

B, The scheme shows the extent of AAV transfection in the WT (n=5) and ephrinA5 (n=5) cases; iThe injection site was reconstructed for each case, and were drawn manually on representative coronal raphe sections (Bregma: -4.60mm) using a different color code for each case.

C, Sagittal mouse brain scheme showing the projections from the DR and MnR to the olfactory bulb (OB) targeting the inner (GCL) or outer (GL) layers respectively.

C', In situ hybridization of ephrinA5 (Efna5) mRNA on OB coronal section. A selective expression of ephrinA5 is observed in the mitral layer (ML). Scale bar=250µm

D-E', Anterogradely labeled axons (td-tomato) and SERT+ fibers in the OB of WT (D, D') and ephrinA5 KO mice (E, E'). Most of the td-tomato were co-labeled with SERT. More co-labeled fibers were detected in the EPL of ephrinA5 -/- mice, compared to WT. Scale bar=50µm.

F-H, Histograms show the fiber densities of anterogradely labeled and SERT-labeled axons. (F) The density of td-tomato fibers was normalized by calculating the EPL/GCL fi-

ber density ratio. The density of 5-HT axons was measured as linear density of SERT labelled axons (fibers/µm) in the EPL (G) and CGL (H) (***p<0.005)

**Figure 7- EphrinA5 expression modulates the DR innervation in forebrain target.**

A, F, Expression of ephrinA5 (Efna5) in the ventromedial hypothalamus (VMH) (A), and the suprachiasmatic nucleus (SCN) (F) in coronal brain section of P5 mice. High level of ephrinA5 were detected in the VL and DM part of VMH. Scale bar=500µm.

B-B", C-C", G-G", H-H', immunofluorescence images show SERT labeling and anterograde labeling of DR in adult in control (B-B", G-G") and ephrinA5 KO mice (C-C", H-H"). Few fibers were detected in VMH and SCN of the control cases whereas labeled fibers were detected in larger amounts in the VMH and SCN of the ephrinA5 KO (see arrows to compare between pictures). Scale bar=100µm (B-C"), 50µm (G-H").

D, E, I, J,) Histograms show the fiber densities anterogradely labeled and SERT+ axons. Fiber density was calculated as pixels per $\mu m^2$ and the data are presented as mean ± SEM, unpaired t test, *p<0.05, **p<0.01 and ***p<0.005.

**Figure 8-Summary diagram.** This scheme shows the expression level of EphA5 in the different 5-HT raphe nuclei, indicated with different shades of green, the maximal being in the DR-V, and lowest in B1, B2. The projections of the DR 5-HT neurons to the amygdala and to the granular cell layer (GCL) of the olfactory bulb are indicated with solid lines. In the ephrinA5 knock out mice, additional projections to the ventromedial hypothalamus (VMH) and to the external plexiform layer (EPL) are visible; these are indicated with dotted lines. High ephrinA5-expression in the mitral cell layer (ML) and the VMH is indicated in orange.

**Table legends**

**Table 1. List of mRNA probes**

**Table 2. List of RT-QPCR primers**

**Table 3. Counts of Tph2-immunopositive and EphA5 expressing neurons and colocalized neurons in different raphe nuclei**

Figures are the mean cell numbers +/- SEM / area obtained from counts done in 3 cases in regions of interest (ROI ) covering the different raphe nuclei (B1 to B9) . All cells (validated by DAPI staining) immunolabeled for Tph2, for EphA5 and double-labeled for Tph2 and EhpA5 were counted in 3 different ROI (dimension 0,225$mm^2$ ) for each structures

886 and for each case and checked for co-localization % of the co-labeled Tph2 neurons is
887 indicated.

888 **Table 4. Counts of Tph2-immunopositive and EphA5 expressing neurons and colo-**
889 **calized neurons in the dorsal raphe (B7) (mean ± SEM, n=3).**

890

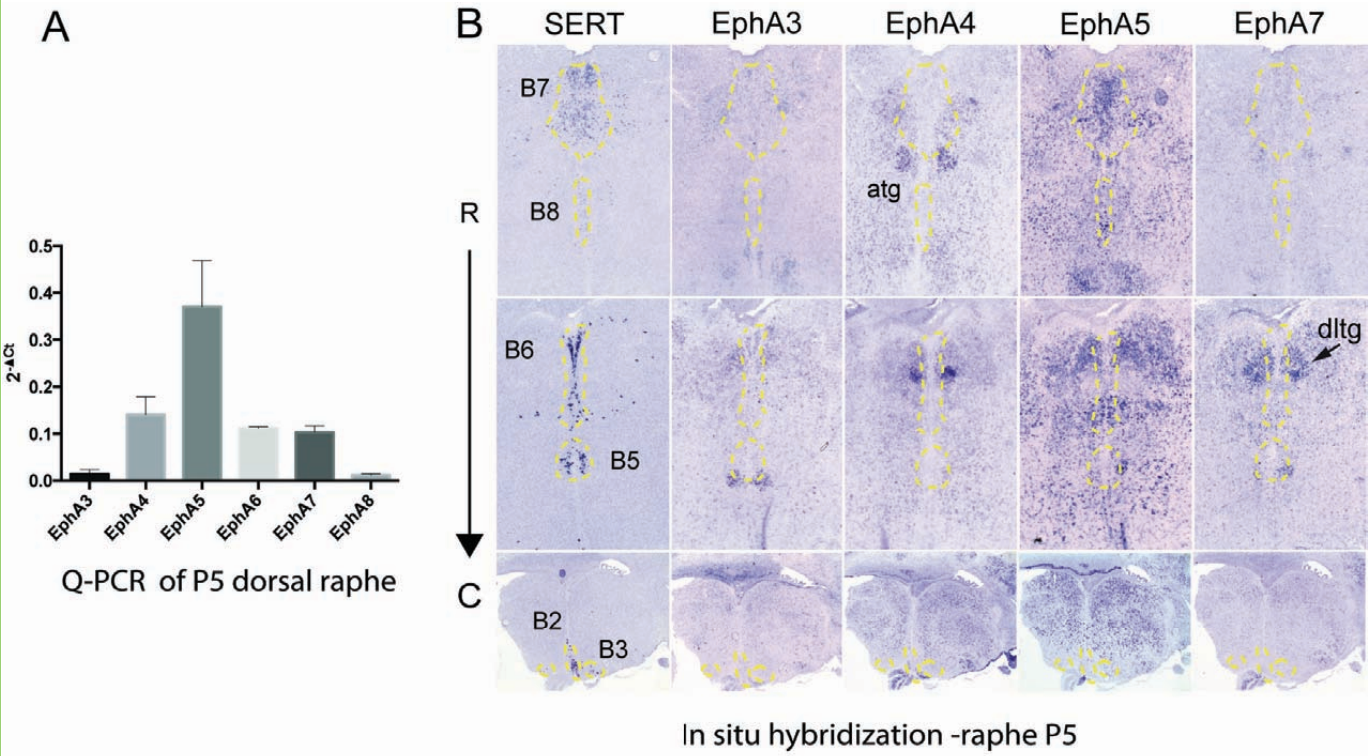

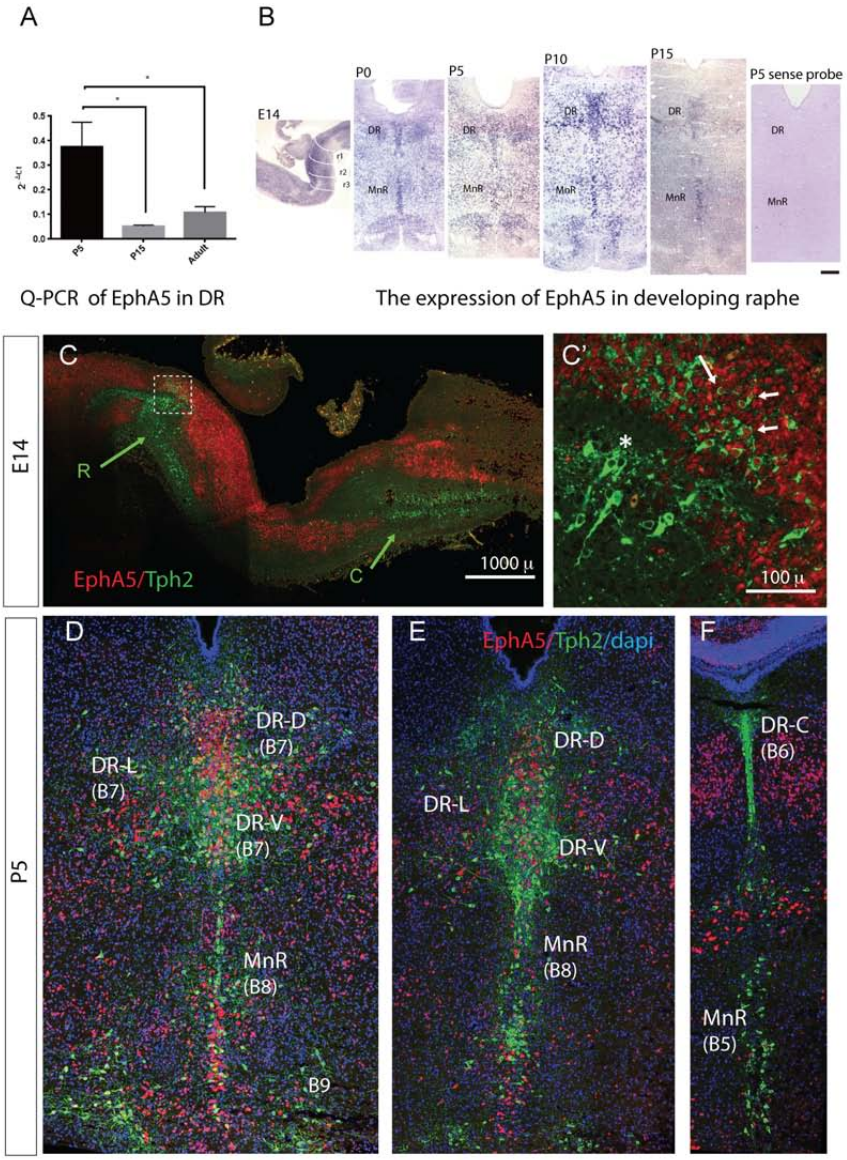

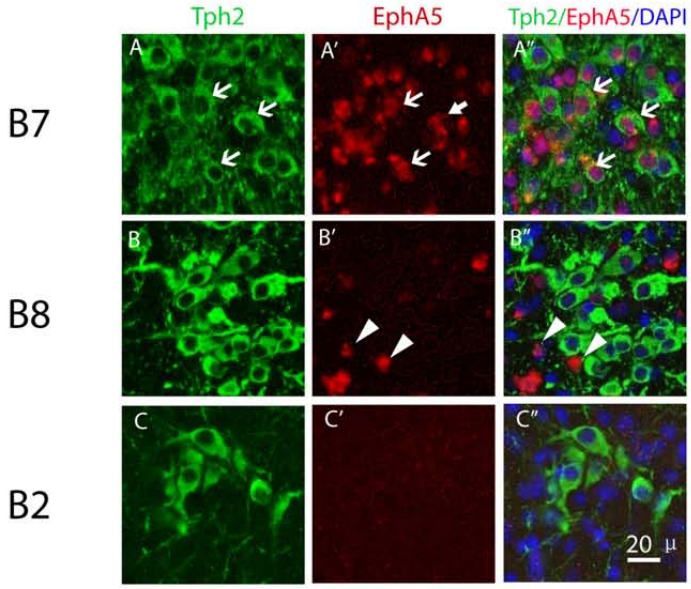


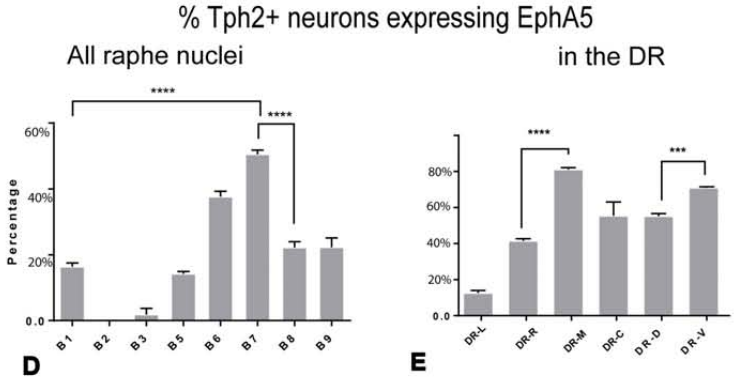

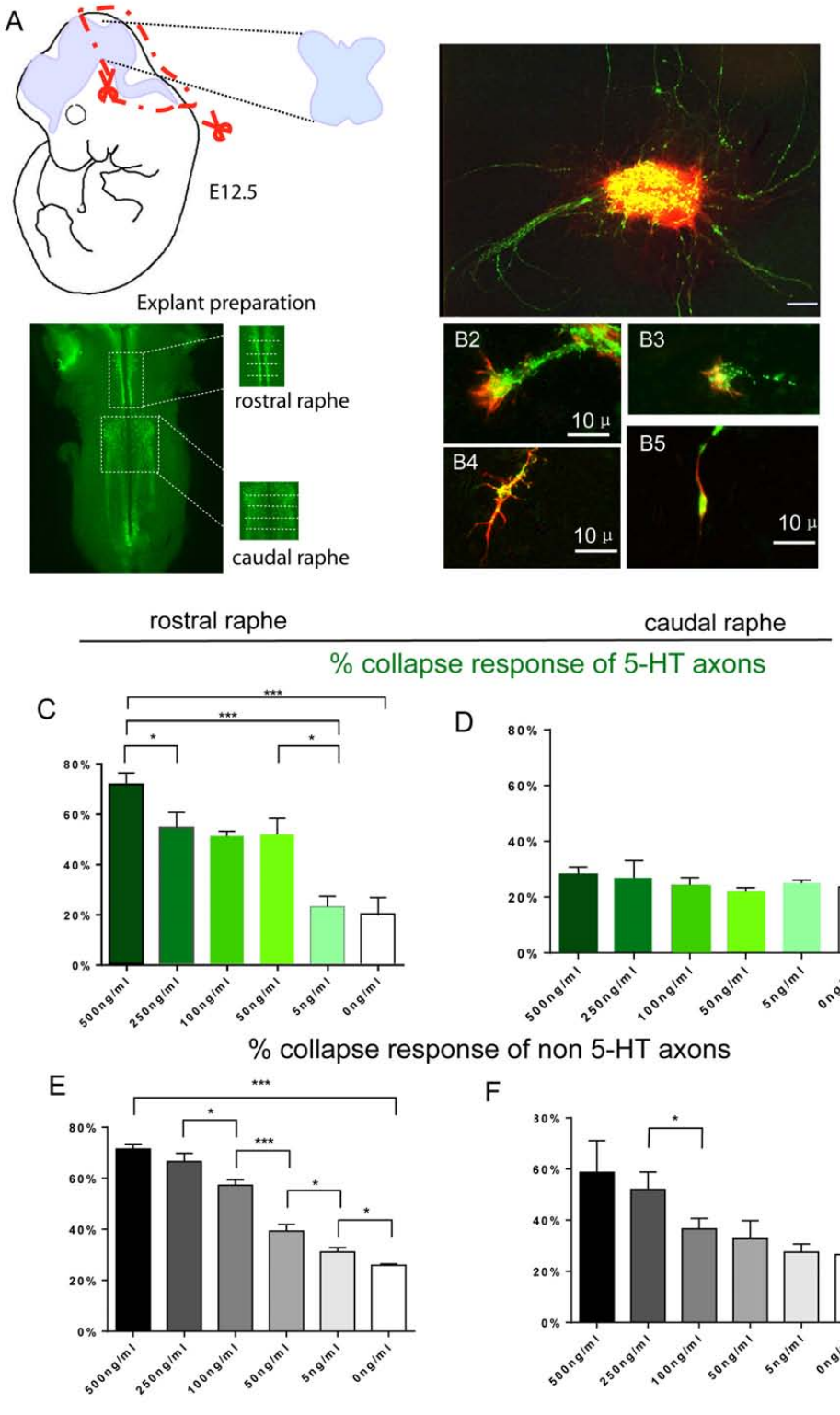

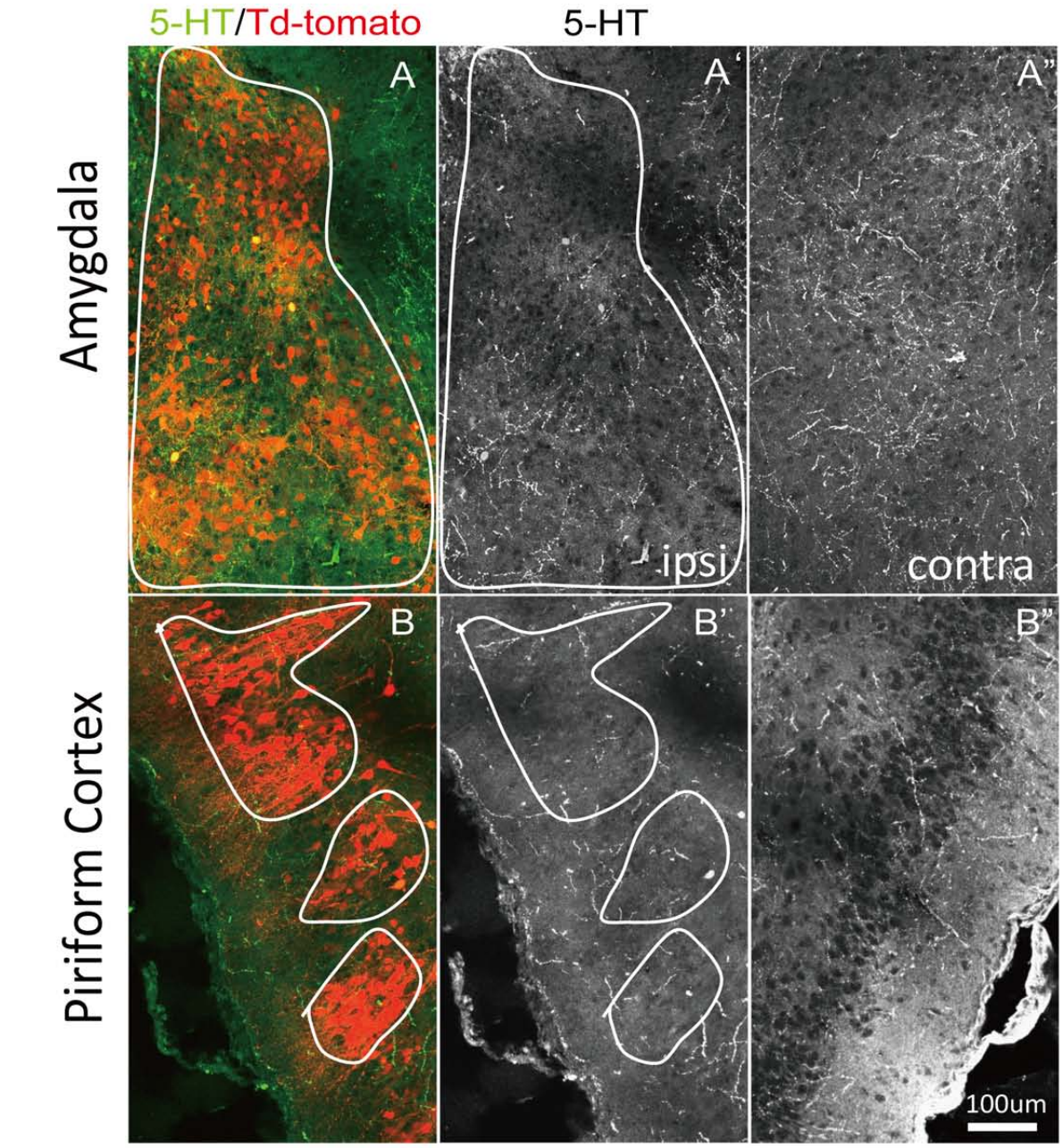


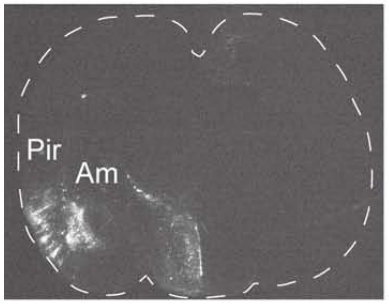


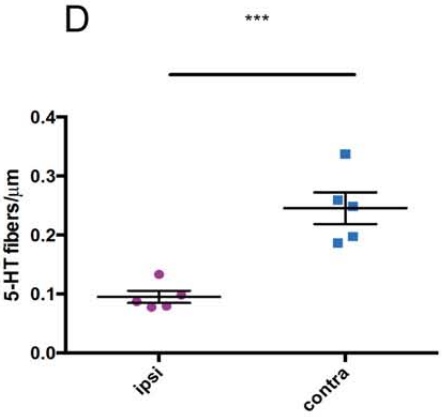


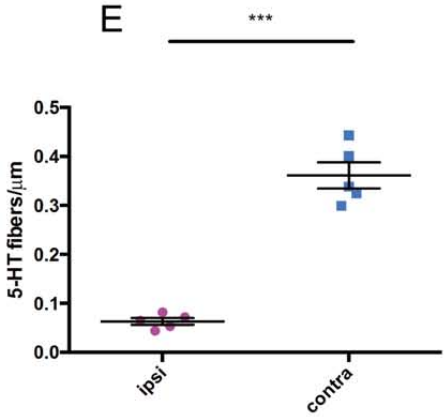

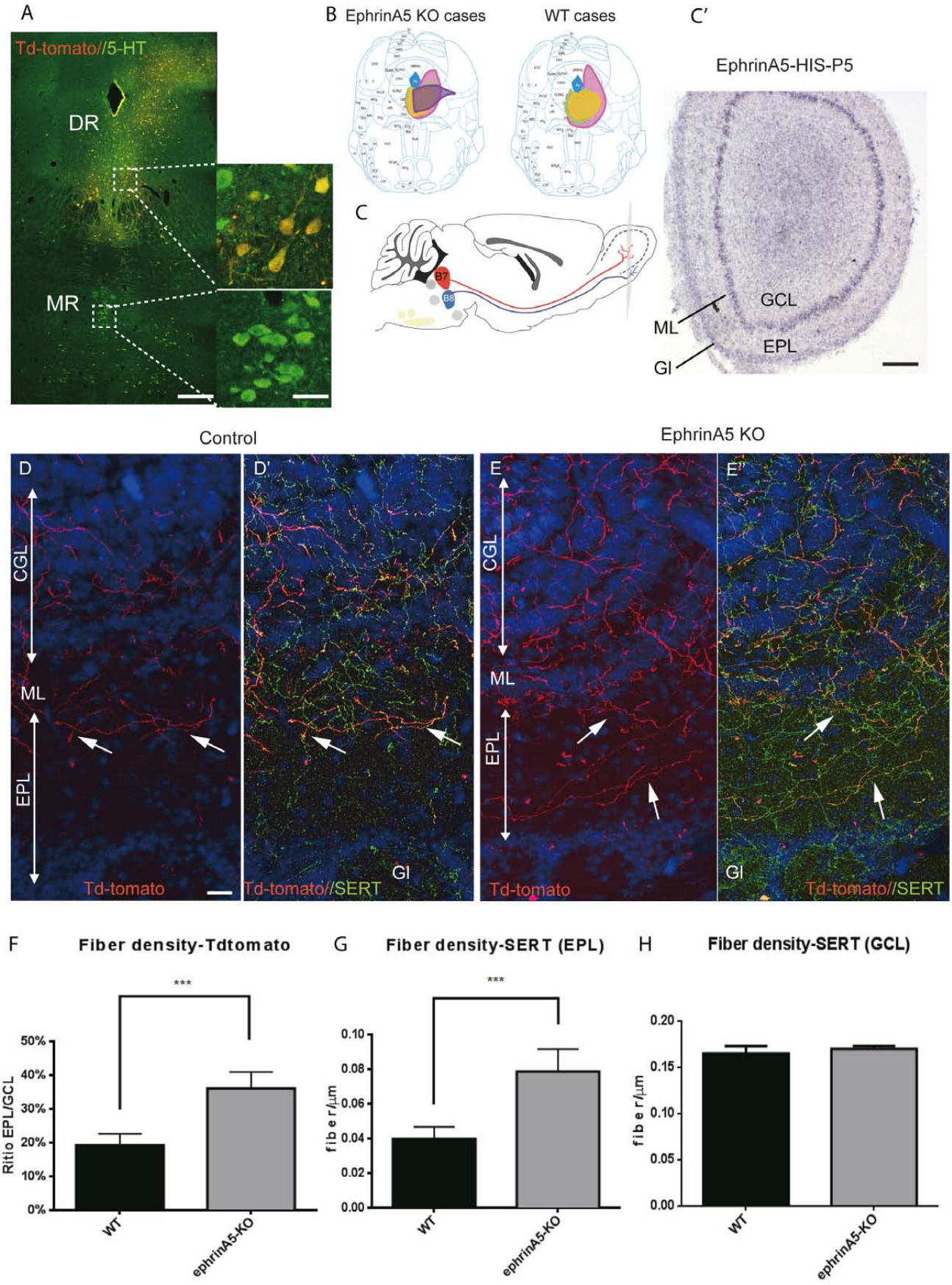

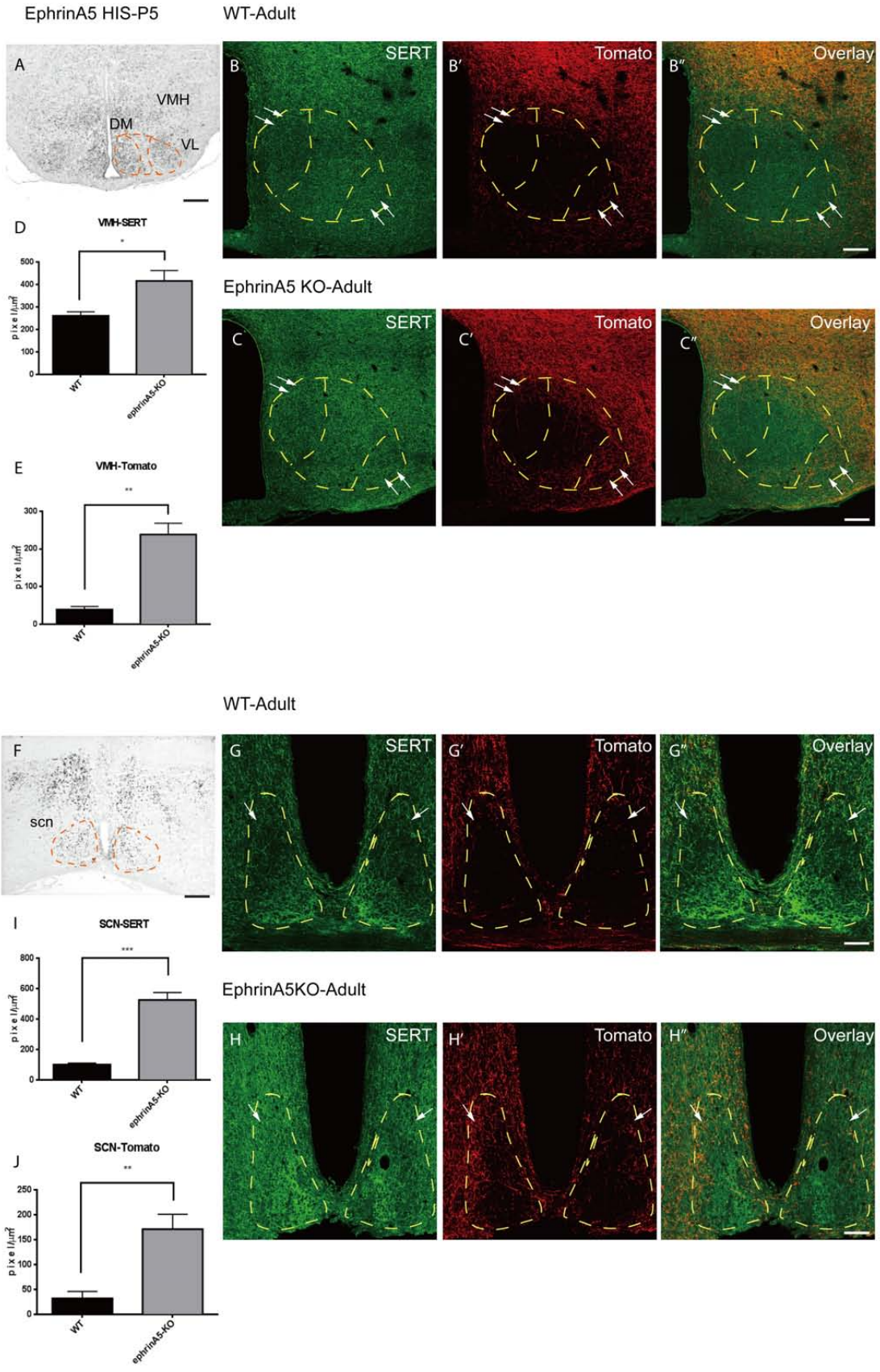

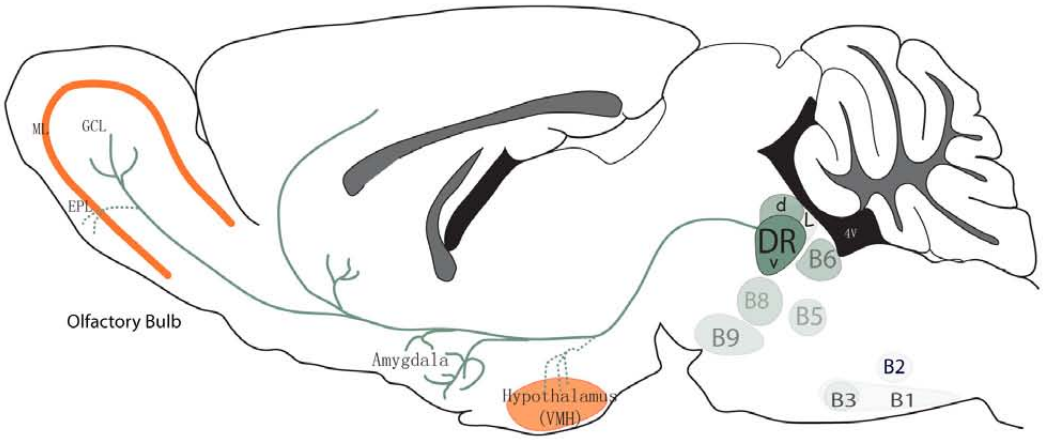

**Table 1 Primers for mRNA probe synthesis**

| | **Restiction enzyme** | | **Polymerase** | |
|---|---|---|---|---|
| | Sense | anti-sense | Sense | anti-sense |
| EphA3 | HindIII | EcoRI | T7 | T3 |
| EphA4 | SacI/SacII | XhoI/BamHI | T7 | T3 |
| EphA5 | XbaI | BamHI | | T7 |
| EphA7 | BamHI | XhoI | T7 | SP6 |
| Efna2 | HindIII | EcoRV | SP6 | T7 |
| Efna3 | XhoI | BamhI | T7 | SP6 |
| Efna5 | HindIII | XbaI | T3 | T7 |

**Table2 RT-QPCR primers**

| | mRNA Variant 1 | Primer info | Forward primer | Reverse primer |
|---|---|---|---|---|
| EphA3 | NM_010140 | Product length 116 | TGCGGGACTGTAACAGCATT | CGTGAACTGATGCTCTCGGA |
| EphA4 | NM_007936 | Product length 90 | GAGGCTCCTGTGTCAACAACT | AGTTGCCAATGGGTACCAGC |
| EphA5 | NM_007937 | Product length 98 | TTGGCTGTTGACCAGTTGGA | GTCCTCCAGGAAGGCTGTTG |
| EphA6 | NM_007938 | Product length 90 | ACTGAAATCCGTGAGGTGGG | GACTGAGACCAGAGCGATGC |
| EphA7 | NM_010141 | Product length 98 | TCCTCCTTAGTCGAGGTCCG | GCCACTCTCCTTCTGCACTG |
| EphA8 | NM_007939 | Product length 95 | CATTGCTTTCCGCACGTTCT | TCCAGTAGGGTCGTTCACCA |

**Table 3 Measures of EphA5-Tph2 co-localization in the B1-B9 cell groups**

| | B1 | B2 | B3 | B5 | B6 | B7 | B8 | B9 |
|---|---|---|---|---|---|---|---|---|
| Tph2+ | 8,2±0,9 | 2,8±0,1 | 7,4±0,9 | 5,1±0,1 | 30,7±1,9 | 11,2±0,9 | 5±0,4 | 7,3±0,5 |
| EphA5+ | 19,3±3,3 | 3,3±1,7 | 2,9±1,5 | 8,9±0,2 | 41,2±2,9 | 23,3±2,2 | 18,9±1,6 | 16,9±0,8 |
| Tph2+/EphA5+ | 1,3±0,2 | 0 | 0,1±0,1 | 0,7±0,1 | 11,5±0,6 | 5,7±0,4 | 1,1±0,1 | 1,6±0,2 |
| % Tph2 colocalized | 16,4± 1% | 0 | 1,8 ±1,9% | 14,3± 0,7% | 37,6%± 1,6% | 50,5± 1,2% | 22,3± 0,2% | 22,3±2,8% |

**Table 4 Measures of EphA5-Tph2 co-localization in the DR cell groups**

| | DR-LW | DR-C | DR-M | DR-R | DR-D | DR-V |
|---|---|---|---|---|---|---|
| Tph2+ | 4,5±0,6 | 17,8±2,3 | 20,2±1,6 | 21±2 | 20,1±2,1 | 17,9±1,8 |
| EphA5+ | 20±1,2 | 20,6±3,6 | 38,3±4,3 | 18,6±3,1 | 32,8±3,5 | 26,2±4,5 |
| Tph2+/EphA5+ | 0,6±0,1 | 7,4±1,1 | 16,4±1,4 | 11,3±0,7 | 11,1±1,4 | 12,7±1,2 |
| % Tph2 colocalized | 12,6% ± 1,5% | 41,5±1,2 | 81,1% ± 1% | 44,4% ± 7,7% | 55,2% ± 1,4% | 70,9% ± 0,6% |

| Line | Data structure | Type of test | Power |
|---|---|---|---|
| a, Qpcr analysis of EphA5 expression during development (Figure 2A) | Homocedacy | One way ANOVA Tukey's multiple comparisons test | 0.7792 |
| b1, Quantification of EphA5-Tph2 co-localization in distinct raphe nucleus (Figure 3D) | Homocedacy | One way ANOVA Tukey's multiple comparisons test | 0.8335 |
| b2, Quantification of EphA5-Tph2 co-localization in dorsal raphe nucleus (Figure 3E) | Homocedacy | One way ANOVA Tukey's multiple comparisons test | 0.7097 |
| c1, Quantification of percentage of collapsed growth cones (Figure C) | Homocedacy | One way ANOVA Tukey's multiple comparisons test | 0.9714 |
| c2, Quantification of percentage of collapsed growth cones (Figure D) | Homocedacy | One way ANOVA Tukey's multiple comparisons test | 0.9783 |
| c3, Quantification of percentage of collapsed growth cones (Figure E) | Homocedacy | One way ANOVA Tukey's multiple comparisons test | 0.266 |
| c4, Quantification of percentage of collapsed growth cones (Figure F) | Homocedacy | One way ANOVA Tukey's multiple comparisons test | 0.934 |
| d1, Quantification of fiber density in amygdala after Efna3 overexpressed (Figure 5D) | Homocedacy | Paired t test (two tailed) | 1 |
| d2, Quantification of fiber density in amygdala after Efna3 overexpressed (Figure 5E) | Homocedacy | Paired t test (two tailed) | 1 |
| e1, Quantification of fiber density WT vs Efna5-/-, OB (Figure 6F) | Homocedacy | Unpaired t test (two tailed) | 1 |
| e2, Quantification of fiber density WT vs Efna5-/-, OB (Figure 6G) | Homocedacy | Unpaired t test (two tailed) | 1 |
| e3, Quantification of fiber density WT vs Efna5-/-, OB (Figure 6H) | Homocedacy | Unpaired t test (two tailed) | 0.052 |

| | | | |
|---|---|---|---|
| f1, Quantification of fiber density WT vs Efna5-/-, VMH (Figure 7D) | Homocedacy | Unpaired t test (two tailed) | 1 |
| f2, Quantification of fiber density WT vs Efna5-/-, VMH (Figure 7E) | Homocedacy | Unpaired t test (two tailed) | 1 |
| g1, Quantification of fiber density WT vs Efna5-/-, SCN | Homocedacy | Unpaired t test (two tailed) | 1 |
| g2, Quantification of fiber density WT vs Efna5-/-, SCN | Homocedacy | Unpaired t test (two tailed) | 1 |

## *Statistical Table*

Statistical Calculations were done with scientific software Graphpad Prism 6, published by GraphPad Software, Inc. CA 92037 USA
Powers of each experiment were calculated by an online power calculator
https://www.anzmtg.org/stats/PowerCalculator